Monthly Notices of the ROYAL ASTRONOMICAL SOCIETY

MNRAS **525,** 5291–5297 (2023) https://doi.org/10.1093/mnras/stad2687
Advance Access publication 2023 September 6

Ultraluminous quasars at high redshift show evolution in their radio-loudness fraction in both redshift and ultraviolet luminosity

Philip Lah [1]★ Christopher A. Onken [1] Ray P. Norris [2,3] and Francesco D'Eugenio [4,5]

[1] *Research School of Astronomy and Astrophysics, Australian National University, Canberra, ACT 2611, Australia*
[2] *Western Sydney University, Locked Bag 1797, Penrith, NSW 2751, Australia*
[3] *CSIRO Space & Astronomy, PO Box 76, Epping, NSW 1710, Australia*
[4] *Kavli Institute for Cosmology, University of Cambridge, Madingley Road, Cambridge, CB3 0HA, UK*
[5] *Cavendish Laboratory, University of Cambridge, 19 JJ Thomson Avenue, Cambridge, CB3 0HE, UK*

Accepted 2023 August 25. Received 2023 August 10; in original form 2023 February 22

ABSTRACT

We take a sample of 94 ultraluminous, optical quasars from the search of over 14 486 deg^2 by Onken et al. in the range 4.4 < redshift < 5.2 and match them against the Rapid ASKAP Continuum Survey (RACS) observed on the Australian Square Kilometre Array Pathfinder (ASKAP). From this most complete sample of the bright end of the redshift ∼5 quasar luminosity function, there are 10 radio continuum detections, of which eight are considered radio-loud quasars. The radio-loud fraction for this sample is 8.5 ± 2.9 per cent. Jiang et al. found that there is a decrease in the radio-loud fraction of quasars with increasing redshift and an increase with increasing absolute magnitude at rest frame 2500 Å. We show that the radio-loud fraction of our quasar sample is consistent with that predicted by Jiang et al.,extending their result to higher redshifts.

Key words: galaxies: quasars: general – radio continuum: galaxies.

1 INTRODUCTION

Quasars were first discovered through their radio emission (Matthews & Sandage 1963; Schmidt 1963). However, it was soon found that the majority of quasars had little or no detectable radio emission (Sandage 1965). Quasars are often classified into two categories: radio-loud and radio-quiet, based on the ratio of their radio to optical flux density. Some authors find a bimodal distribution for radio-loud and radio-quiet quasars (Kellermann et al. 1989; Miller, Peacock & Mead 1990; Visnovsky et al. 1992; Goldschmidt et al. 1999; Ivezić et al. 2002, 2004b; White et al. 2007). Others find no evidence for such a distribution (Lacy et al. 2001; Cirasuolo et al. 2003; Singal et al. 2011; Baloković et al. 2012; Singal et al. 2013; Macfarlane et al. 2021).

The spectral energy distributions of radio-loud and radio-quiet quasars are very similar (Elvis et al. 1994; de Vries, Becker & White 2006; Richards et al. 2006; Shang et al. 2011; Shankar et al. 2016), differing only in the X-ray and radio bands. At low redshift, the vast majority of radio-loud quasars are hosted by giant elliptical galaxies, while radio-quiet quasars are found to be hosted by both elliptical and spiral galaxies (Floyd et al. 2010; Tadhunter 2016; Rusinek et al. 2020). At higher redshifts, radio-loud quasars have higher star formation than radio-quiet quasars (Kalfountzou et al. 2012), which is consistent with their role as the progenitors of the low-redshift, high-mass ellipticals. Radio-loud quasars are found in denser environments as well as having much more massive dark matter haloes and higher stellar masses than radio-quiet quasars (Mandelbaum et al. 2009; Shen 2009; Donoso et al. 2010; Wylezalek et al. 2013; Rees et al. 2016; Retana-Montenegro & Röttgering 2017).

Quasars are thought to be triggered by the high accretion associated with galactic mergers (Hopkins et al. 2006). Most of the radio-loud quasars and some radio-quiet quasars are thought to be due to mergers of elliptical galaxies with disc galaxies, while the remaining radio quiet quasars are due to the mergers of two disc galaxies (Shen 2009; Bessiere et al. 2012; Treister et al. 2012). The dependency of the type of galaxy merger with the radio properties of the quasar can be tested by comparing the fraction of radio-loud quasars with the cosmic history of the different types of mergers. The fraction of elliptical-spiral mergers decreases with increasing redshift, while the fraction of spiral–spiral mergers increases with redshift as seen in semi-analytical models (Khochfar & Burkert 2003) and in observations (Lin et al. 2008). This suggests that the radio-loud fraction would decrease with increasing redshift.

Indeed, many authors have shown that the radio-loud fraction does decrease with increasing redshift (Peacock, Miller & Longair 1986; Miller et al. 1990; Schneider et al. 1992; Visnovsky et al. 1992; La Franca et al. 1994), although some authors have shown no evolution with redshift (Goldschmidt et al. 1999; Stern et al. 2000; Ivezić et al. 2002). Many authors have shown that the radio-loud fraction increases with optical luminosity (Visnovsky et al. 1992; Padovani 1993; Goldschmidt et al. 1999), while a few authors find no such trend (Stern et al. 2000; Ivezić et al. 2002), and a few authors show the radio-loud fraction increasing with luminosity (Hooper et al. 1995; Bischof & Becker 1997). These early results were often complicated by small sample sizes and the complex interplay of redshift, luminosity, and survey flux limits.

Of particular relevance to this paper is the work by Jiang et al. (2007), where they used 30 000 optically selected quasars from the

★ E-mail: philip.lah@anu.edu.au

Sloan Digital Sky Survey matched to the Faint Images of the Radio Sky at Twenty-Centimeters (FIRST) radio survey to examine the properties of the radio fraction of quasars. They found that the radio-loudness fraction of quasars is a function of both redshift and rest frame 2500 Å luminosity, with the fraction decreasing with redshift and increasing with luminosity. The work of Jiang et al. (2007) did not extend out to the redshifts probed by our work, reaching only out to redshift ∼4.6. The conclusions of Jiang et al. (2007) were supported by the later work of Kratzer & Richards (2015); Rusinek-Abarca & Sikora (2021).

Yang et al. (2016) found for luminous quasars at 4.7 < redshift < 5.4 that the radio-loud fraction may evolve with optical luminosity but that the fraction may not decline as rapidly with increasing redshift as measured by Jiang et al. (2007). Bañados et al. (2015), in a sample of quasars at redshift >5.5, found that there appeared to be no evolution in the radio-loud fraction at these redshifts, as does Liu et al. (2021) for a similar redshift sample.

Ultraluminous quasars at high redshift are extremely rare, but these objects are of particular interest as the early Universe is the era in which supermassive black holes undergo their most dramatic and least explained growth. Ultraluminous quasars are difficult to find as the candidate lists are swamped by the tail-end distribution of cool, red stars from within our own Galaxy. To find these rare objects, Onken et al. (2022) used photometry from the SkyMapper Southern Survey (SMSS) Data Release 3 (Wolf et al. 2018; Onken et al. 2019), the 2 Micron All-Sky Survey (2MASS; Skrutskie et al. 2006), the VISTA Hemisphere Survey (VHS) Data Release 6 (McMahon et al. 2013), the VISTA Kilo-degree Infrared Galaxy (VIKING) Survey Data Release 5 (Edge et al. 2013), AllWISE (Wright et al. 2010), and the CatWISE2020 Catalog (Marocco et al. 2021). (VISTA is the Visible and Infrared Survey Telescope for Astronomy and *WISE* is the *Wide-field Infrared Survey Explorer*). In addition, they used proper motions from the *Gaia* Data Release 3 (Gaia Collaboration et al. 2021) to remove stars from their candidate lists. Spectroscopic follow-up was then done with the Australian National University (ANU) 2.3-m telescope to confirm the targets as quasars and to obtain precise redshifts. This yielded a sample of redshift ∼5 quasars with unprecedented completeness at the bright end.

In this paper, we have matched the quasars from Onken et al. (2022) to the new Rapid ASKAP Continuum Survey (RACS; McConnell et al. 2020; Hale et al. 2021) to measure the evolution of the radio-loud fraction for these objects, as seen in previous work (e.g Jiang et al. 2007).

In Section 2, the quasar data from the optical and infrared combined with the radio data is analysed to determine the radio-loud fraction of the sample. In Section 3, the completeness of the sample in both radio and optical mode is examined. In Section 4, we discuss the radio-loud fraction, and its evolution with redshift and optical rest frame luminosity. In Section 5, the conclusions from this work are summarized.

2 ANALYSIS

Onken et al. (2022) searched for ultraluminous quasars at redshift greater than 4.4 over 14 486 deg^2 of the whole sky from Dec <+2°, Galactic latitude $|b| > 15°$ and excluding some regions around the Magellanic Clouds and other nearby galaxies in the local group as well as regions around bright stars. Quasar candidates were limited to those with a SkyMapper z-band zPSF <19.5 AB magnitude. Cross-matches were made with the large-area surveys *Gaia*, WISE, and VISTA and candidates with a neighbour within 5 arcsec were removed. The following selection criteria were used to remove contamination by cool, red stars, and lower redshift quasars:

$$
\begin{aligned}
&0.8 < G - Rp < 1.8\\
&1.8 < Bp, c - Rp\\
&0.9 < gPSF - rPSF\\
&0.7 < J - K < 1.8\\
&1.5 < J - W1 < 3\\
&0.2 < W1 - W2 < 1.1\\
&2.3 < W1 - W3 < 4.7\\
&0 < (J - K) + (Bp, c - Rp) - (zPSF - J) - 1.8\\
&0 < (J - W1) - 1.4(zPSF - J) + 0.1\\
&0 < 0.6 - 0.5(rPSF - iPSF) - (G - rPSF),
\end{aligned}
\tag{1}
$$

where *gPSF*, *rPSF*, and *zPSF* are passbands from SkyMapper; *G*, *Bp*, *c*, and *Rp* are passbands from *Gaia*; *J*, *H*, and *K* are passbands from VHS and VIKING; *W*1 and *W*2 are passbands from CatWISE and *W*3 is a passband from AllWISE. *Bp*, *c* is corrected for magnitude-dependent biases. The next criterion was that the *Gaia* proper motions and parallaxes for the objects were consistent with zero within the errors (2σ). The quasar candidates were then followed up with spectroscopic observations with the ANU 2.3-m telescope. Known quasars from Milliquas v7.1 (Flesch 2015) in the search area were added to the quasar sample.

This quasar list was matched to the radio continuum sources from RACS from Hale et al. (2021). RACS was observed at a frequency of 887.5 MHz with a bandpass of 288 MHz. The RACS sample from Hale et al. (2021) covers a Declination range from −80° to + 30° excluding Galactic latitudes $|b| < 5°$, resulting in a good match to the region covered by Onken et al. (2022). RACS has a resolution of 25 arcsec and a median RMS ∼0.3 mJy beam^{-1}. There are ∼2.1 million radio continuum sources in RACS.

The sample of optical quasars from Onken et al. (2022) chosen to match to RACS was limited to a range 4.4 < redshift < 5.2, where the sample is most complete. A cut-off in the SkyMapper $z$band of AB magnitude <18.7 was used, for which the sample was 78 per cent complete (Onken et al. 2022). The enhanced completeness relative to the study of Yang et al. (2016) (∼55 per cent) is primarily due to the recent availability of *Gaia* astrometry, which allowed further exploration of the ($W1 - W2$) colour space without suffering from overwhelming stellar contamination. Below this magnitude cut, the sample's incompletness increases greatly. Incompleteness is calculated from the variation of Skymapper z-band number counts with magnitude and spectroscopic follow-up of candidate quasar objects. This gave an optical quasar sample of 94 quasars. These optical quasars were matched to the objects in RACS with a maximum matching radius of 10 arcsec. There were 10 matched objects, with the maximum matching radius being 2.83 arcsec, and most being less than 1 arcsec.

The definition for radio loudness used in this paper is that used by Jiang et al. (2007), which is based on earlier work by Stocke et al. (1992). This differs from other definitions, as it is defined in the ultraviolet rather than the optical (e.g. at 4400 Å used by Kellermann et al. (1989) from the original paper on radio loudness). The advantage of using the ultraviolet is that the observed wavelength for high redshift quasars is lower, making it easier to measure.

The radio loudness has the form:

$$
R = \frac{f_{5000\,\mathrm{MHz}}}{f_{2500\,\text{Å}}}. \tag{2}
$$

Where $f_{5000\,\mathrm{MHz}}$ is the flux density of the quasar at rest frame 5000 MHz and $f_{2500\,\text{Å}}$ is the flux density at rest frame 2500 Å.

Table 1. The properties of the quasars with radio continuum detections in RACS. In the last two columns, a '–' means that the object is outside the area covered by the surveys and and a '∗' meant that the source was not detected in the survey.

R	SkyMapper Southern Sky Survey ID	RA (°)	DEC (°)	Redshift	z mag	mag 2500	mag 2500 abs	flux RACS (mJy)	flux NVSS (mJy)	flux VLASS (mJy)
5.2	035504.86–381142.5	58.77027	− 38.19514	4.545	17.44	19.04	− 29.11	2.51	2.2	2.89
6.5	151443.82–325024.8	228.68260	− 32.84022	4.810	17.85	19.09	− 29.20	3.24	∗	∗
15.9	232952.75–200038.7	352.46985	− 20.01085	5.030	18.45	19.92	− 28.48	3.88	∗	∗
33.0	145147.04–151220.1	222.94603	− 15.20561	4.763	17.12	18.71	− 29.56	22.94	28.5	44.82
55.9	013127.34–032059.9	22.86391	− 3.34998	5.196	18.03	19.39	− 29.10	23.19	31.4	49.78
93.9	013539.28–212628.2	23.91370	− 21.44118	4.940	17.74	19.21	− 29.15	43.23	25.3	31.48
207.4	043923.20–020701.6	69.84667	− 2.11710	4.400	18.68	19.96	− 28.10	41.37	43.3	50.58
264.0	033951.43–473959.9	54.96432	− 47.66662	4.450	18.65	20.59	− 27.51	29.97	–	–
556.3	052506.17–334305.6	81.27573	− 33.71823	4.417	18.18	19.62	− 28.45	152.02	188.3	104.79
745.2	032444.28–291821.0	51.18452	− 29.30586	4.622	17.93	19.58	− 28.61	224.03	236.5	161.21

At the redshifts of the quasar sample, the redshifted 2500 Å is close to the J and H bands (J, H, and K are Vega magnitudes and come from the VHS and VIKING surveys). At the average redshift = 4.67 for the quasar sample, 2500 Å is observed at 1.42 μm (J band is at 1.22 μm and H is at 1.63 μm). To find the flux density at redshifted 2500 Å, the spectral index was calculated using J and H band (after a minor correction for interstellar foreground extinction using the map from Schlegel, Finkbeiner & Davis (1998)) using the equation:

$$\alpha = \frac{\log(S1/S2)}{\log(\nu 1/\nu 2)}, \quad (3)$$

where S1 and S2 are the flux densities at the frequency of interest and $\nu 1$ and $\nu 2$ are the frequencies of interest. The spectral index was then used to estimate the flux density at 2500 Å, including a 1 + redshift cosmological correction. In the cases where there was no J band due to a lack of coverage by the surveys (one object in the radio detections), a similar estimation was done using H band and K band (2.19 μm) instead and then extrapolating to the redshifted 2500 Å magnitude. In general where J, H, and K bands were all available, the value from his extrapolation from K band was close to the interpolated value from J and H bands, so doing the extrapolation is unlikely to significantly bias the results.

At the redshifts of the quasar sample, the redshifted 5000 MHz is close to the RACS observing frequency of 887.5 MHz. At the average redshift = 4.67 for the quasar sample, 5000 MHz is observed at 880 MHz. To estimate the flux density at exactly 5000 MHz an $\alpha = -0.5$ was used for the quasars, which is the same as used by Jiang et al. (2007), so that our measurements would be as similar to theirs as possible. A spectral index of $\alpha = -0.5$ is typical for quasars (e.g. Ivezić et al. 2004a).

The calculated radio loudness R along with the absolute AB magnitude at rest frame 2500 Å for the quasars with radio detections are shown in Table 1. Here, we define radio-loud as meaning $R > 10$, which is the canonical value used by Kellermann et al. (1989) and others. Of the 10 quasars with radio detections, eight are radio-loud using this definition.

Also in Table 1 are the NRAO VLA Sky Survey (NVSS; Condon et al. 1998) and VLA Sky Survey (VLASS; Gordon et al. 2021) flux densities for the quasars where they are available. (NRAO is the National Radio Astronomy Observatory and VLA is the Very Large Array). Both surveys only extend down to Declination −40° so there is an incomplete overlap in the quasar sample. The frequency of observation of NVSS is ∼1400 MHz, and the survey has a resolution of 45 arcsec. NVSS has a flux density limit of ∼2.5 mJy beam^{-1}. A maximum matching radius of 15 arcsec was used to match NVSS to the optical quasars. The worst match with the quasar sample for NVSS is 13.5 arcsec away, the next being 1.15 arcsec. The frequency of observation of VLASS is 3000 MHz, and the survey has a resolution of 2.5 arcsec. VLASS has a median RMS sensitivity of 0.128 mJy beam^{-1}. A maximum matching radius of 1.5 arcsec was used to match VLASS to the optical quasars. The worst match with the quasar sample was a matching radius of 1.09 arcsec. For the RACS-detected sample, one object is not in the sky coverage of NVSS and VLASS and two objects were not detected by the surveys.

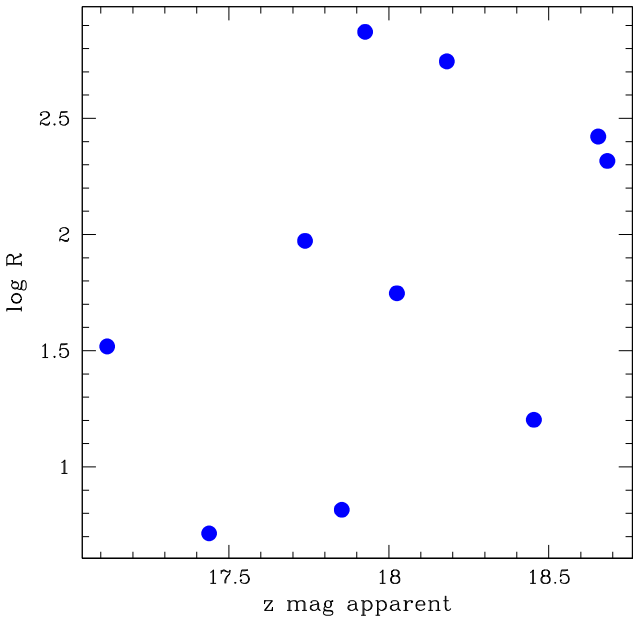

Figure 1. The log of radio loudness of the radio detected quasars versus their apparent z-band magnitude. There is no correlation visible.

3 SAMPLE COMPLETENESS

The optical quasar sample is 78 per cent complete with a SkyMapper $z$magnitude <18.7 (Onken et al. 2022). There is no correlation between radio loudness and z magnitude for the sample (see Fig. 1). Therefore in the missing 22 per cent of quasars, it is reasonable to assume that there is the same ratio of radio-loud quasars as in the 78 per cent, though it should be noted that we are dealing with small number statistics. So in order to reach 100 per cent completeness, one can scale up both the radio detections and the total quasar sample by

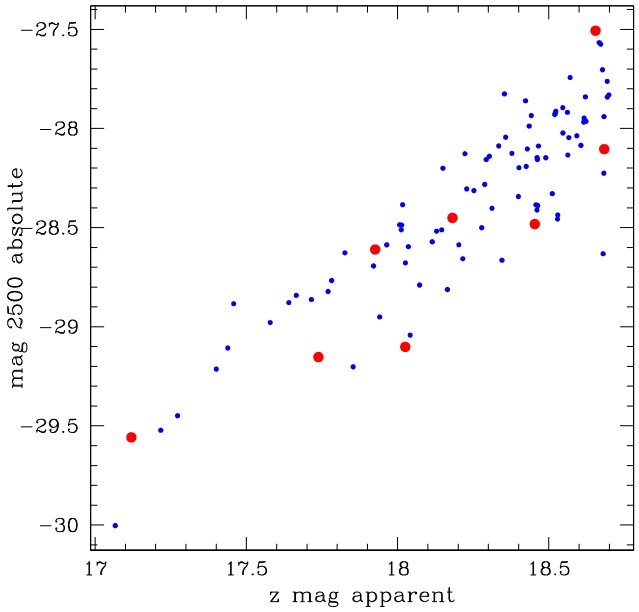

Figure 2. The absolute magnitude at rest frame 2500 Å for all the optical quasars in the sample plotted against their $z$apparent magnitude. The larger, red points are the radio-loud quasars.

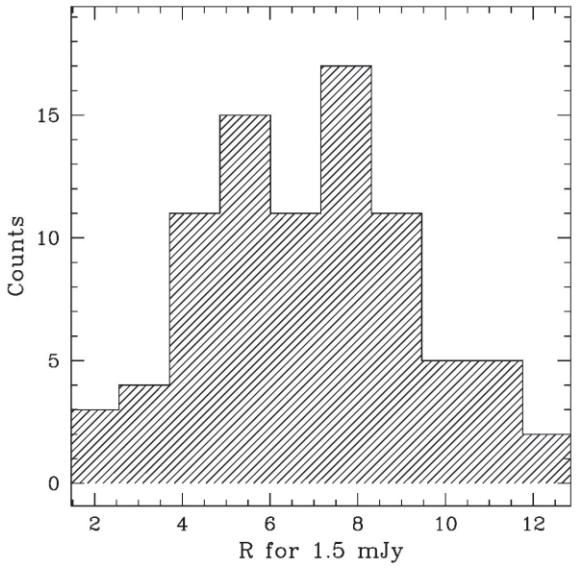

Figure 3. Radio loudness for the quasars without radio detections assuming that the quasars all have a RACS radio flux density of 1.5 mJy (5 times the median RMS of RACS). Radio loud quasars have $R > 10$.

the same amount, which will leave the radio-loud fraction, the ratio of these two quantities, the same.

Fig. 2 shows the absolute magnitude at rest frame 2500 Å for all the optical quasars in the sample plotted against their $z$apparent magnitude. What one can immediately notice is that there is a strong correlation between the absolute magnitude at rest frame 2500 Å and the apparent $z$magnitude. Thus, the cut-off at z-band magnitude of 18.7 can roughly be translated to a cut in the absolute magnitude at rest frame 2500 Å. This means that we are not missing a large number of quasars by using this cut at z-band magnitude of 18.7 rather than a cut in absolute magnitude. Only a few quasars may be missing, which will have the effect of decreasing the measured radio-loud fraction by a small amount.

Fig. 3 shows the radio loudness for the quasars without radio detections, assuming that the quasars all have a RACS radio flux density of 1.5 mJy (5 times the median RMS of RACS), which would therefore have been detected in RACS. The fact that most of the quasars with this assumed flux density are below the cut-off for being radio-loud ($R = 10$) means that we are not missing a large number of radio-loud quasars in our sample due to the RACS flux density limit.

4 RESULTS

The number of radio-loud quasars in the sample is 8 out of a total of 94, which gives a radio-loud fraction of 8.5 ± 2.9 per cent. A binomial distribution was used to determine the error on this fraction. To see if there was any evolution based on this fraction, the value was compared to the work of Jiang et al. (2007). They looked at 30 000 optically selected quasars from the Sloan Digital Sky Survey matched to the FIRST radio survey. From this data, they have the radio-loud fraction as a function of both redshift and optical luminosity as given below:

$$\log\left(\frac{\mathrm{RLF}}{1-\mathrm{RLF}}\right) = b_0 + b_z \log(1+z) + b_{\mathrm{M}}(M_{2500}+26), \qquad (4)$$

where RLF is the radio-loud fraction, z is the redshift, M_{2500} is the absolute magnitude at 2500 Å, $b_0 = -0.132 \pm 0.116$, $b_z = -2.052 \pm 0.261$, and $b_{\mathrm{M}} = -0.183 \pm 0.025$. The work of Jiang et al. (2007) only applies up to a redshift limit of ∼4.0, so our sample would be extrapolating their equation.

The left-hand panel of Fig. 4, using the equation of Jiang et al. (2007) shows the radio-loud fraction as a function of redshift at $M_{2500} = -28.38$, the average of the quasar sample. The light blue is the error on this function. The black point is the radio-loud fraction from our quasar sample at the average redshift. The black lines cover the range of redshifts covered in our sample with the dotted lines showing the range of the error. As can be seen, the function from Jiang et al. (2007) and the value from our work lie within 1σ of each other. This indicates that our data is consistent with the equation of Jiang et al. (2007) in showing that for increasing redshift, the radio-loud fraction decreases for ultraluminous quasars.

The right-hand panel of Fig. 4, using the equation of Jiang et al. (2007), shows the radio-loud fraction as a function of M_{2500} at redshift = 4.67, the average of the quasar sample. The light blue is the error on this function. The black point is the radio-loud fraction from our quasar sample at the average M_{2500}. The black lines cover the range of M_{2500} covered in our sample with the dotted lines showing the range of the error. As can be seen, the function from Jiang et al. (2007) and the value from our work lie within less than 1σ of each other. This indicates that our data is consistent with the equation of Jiang et al. (2007) in showing that for increasing optical luminosity the radio-loud fraction increases for ultraluminous quasars.

One obvious criticism of this result is that we are using a rather large absolute magnitude range in our sample of $M_{2500} = -30.00$ to -27.51 to do our comparison. If we break the magnitude range into two bins ($M_{2500} = -30.00$ to -28.5 and $M_{2500} = -28.5$ to -27.5), we get four and five radio loud quasars out of 35 and 59 optical quasars, respectively. This gives a radio-loud fraction of 11.4 ± 5.4 per cent for the brighter range and 8.5 ± 3.6 per cent for the fainter range, both of which are still in agreement with the equation of Jiang et al. (2007).

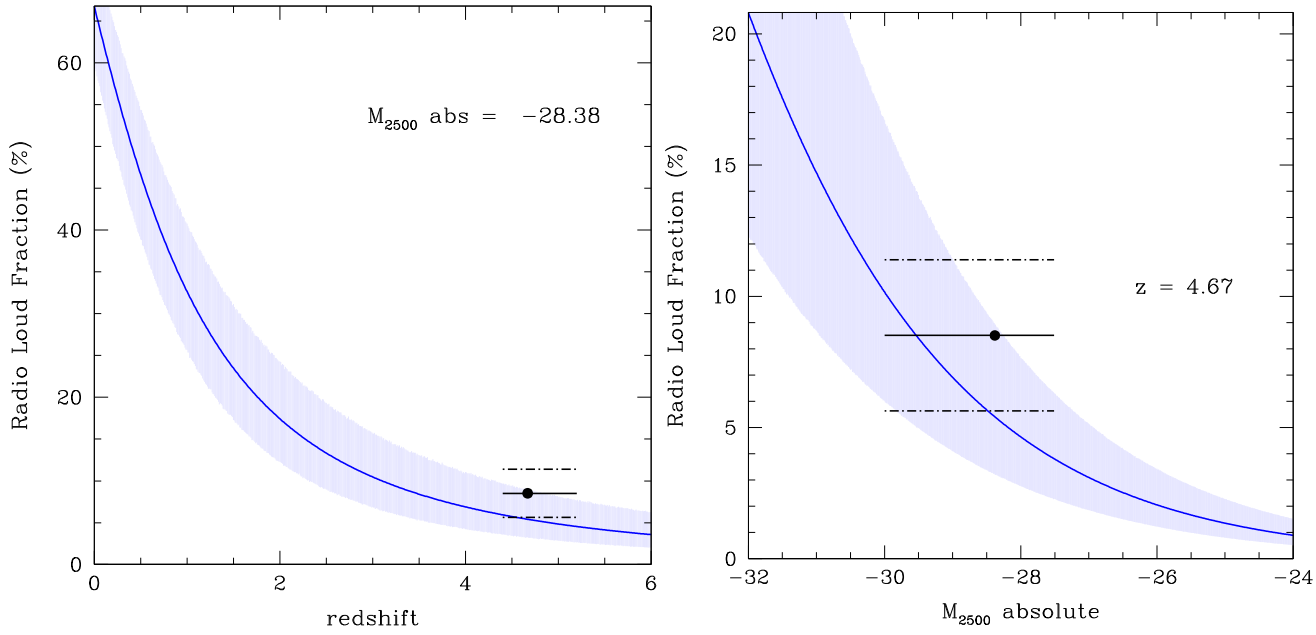

Figure 4. The left-hand panel, using the equation of Jiang et al. (2007), shows the radio-loud fraction as a function of redshift at $M_{2500} = -28.38$, the average of the quasar sample. The light blue is the error on this function. The black point is the radio fraction from our quasar sample at the average redshift. The black lines show the range of redshifts covered in our sample with the dotted lines showing the range of the error. The right-band panel, using the equation of Jiang et al. (2007), shows the radio-loud fraction as a function of absolute magnitude M_{2500} at redshift = 4.67, the average of the quasar sample. The light blue is the error on this function. The black point is the radio fraction from our quasar sample at the average M_{2500}. The black lines cover the range of M_{2500} covered in our sample with the dotted lines showing the range of the error.

Table 2. The radio loud fraction of high redshift quasars from the literature with their redshift ranges and the minimum absolute 2500 mag of their sample.

Source	Radio loud fraction (per cent)	Redshift min	Redshift max	Min mag 2500 abs
This work	8.5 ± 2.9	4.4	5.2	−27.5
Yang et al. (2016)	7.1 ± 2.6	4.7	5.4	−27.0
Bañados et al. (2015)	$8.1^{+5.0}_{-3.2}$	5.5	6.4	−26.9
Liu et al. (2021)	7.1 ± 2.7	5.5	6.5	−25.8

It is known that few galaxies at redshifts greater than ∼4 resemble present-day spiral or elliptical galaxies (Beckwith et al. 2006), and that giant ellipticals or their progenitors are the main source of radio-loud quasars (Floyd et al. 2010; Rees et al. 2016; Tadhunter 2016; Rusinek et al. 2020). If these galaxies represent a smaller fraction of galaxies at these redshifts, it suggests that the radio-loud fraction of quasars should also decrease. Thus, our observed evolution of the radio-loud fraction confirms current models of galaxy evolution.

Table 2 shows the radio-loud fractions for quasars in the literature for high redshift samples. These values have been plotted in Fig. 5 along with the Jiang et al. (2007) function taken at M_{2500} absolute magnitude −28.38, the average of this work's quasar sample. The values from Liu et al. (2021) come from their luminous sample, which has a magnitude limit one magnitude fainter than the other samples. It is also their all-radio sample value. Taken as a whole, these literature values indicate that at the magnitudes they probe there is little evidence for evolution in the radio-loud fraction beyond redshift 5 though there is still reasonable agreement with the function of Jiang et al. (2007). However, it should be noted that the Jiang et al. (2007) function presented in the figure moves from $4.8^{+3.2}_{-1.9}$ per cent at redshift = 5 to $3.6^{+2.8}_{-1.5}$ per cent at redshift = 6. These values are consistent with no change therefore at these redshifts, there is little evidence for evolution, even from the (extrapolated) function of Jiang et al. (2007). Larger differences between the literature values and the function of Jiang et al. (2007) are seen at a fainter M_{2500} absolute value, which is particularly relevant for the Liu et al. (2021) sample.

It is not clear why the radio-loud fraction appears flat near redshift = 6. This is unexpected, as the number and type of galaxies that usually host radio-loud quasars (ellipticals and their progenitors) are still decreasing at these redshifts. This suggests a process that is affecting the radio properties of these distant quasars. For example, since redshift = 6 is approximately the end of the epoch of reionization, perhaps the gas supply for quasars is larger (or maybe just denser and more neutral) in this era so that quasars do not have to rely solely on mergers to support their radio emission. More research needs to be done in this area, both in larger and deeper quasar surveys at these redshifts and in theoretical models that predict the radio loudness fraction of quasars at these redshifts.

5 CONCLUSION

A sample of 94 ultraluminous optical quasars from Onken et al. (2022) in the range 4.4 < redshift < 5.2, with z-band magnitude <18.7, were matched against the radio continuum survey of RACS. Ten quasars had radio detections in RACS, of which eight are

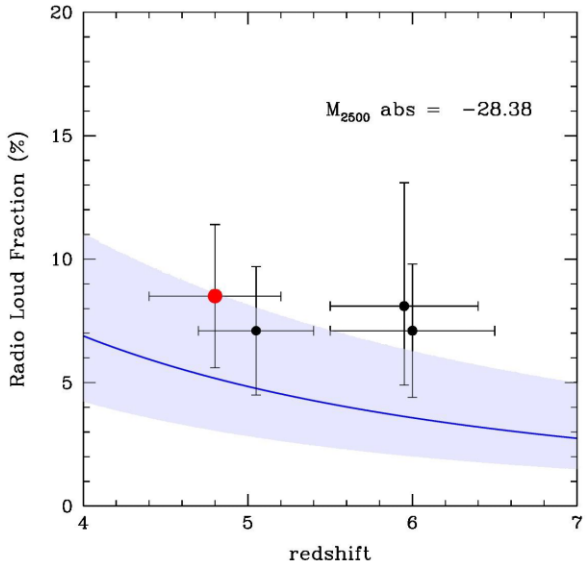

Figure 5. The radio-loud fraction of high-redshift quasars from the literature. The values for each can be found in Table 2. The value for this paper is the large red point. The blue line with the error range around it is the value from the Jiang et al. (2007) function taken at M_{2500} absolute magnitude −28.38, the average of this work's quasar sample.

considered to be radio-loud. The sample thus has a radio-loud fraction of 8.5 ± 2.9 per cent. Jiang et al. (2007) modelled the radio-loud fraction as a function of redshift and absolute magnitude at rest frame 2500 Å. The radio-loud fraction we measure is consistent with an extrapolation of this function showing the predicted decrease with redshift and an increase with absolute magnitude.

ACKNOWLEDGEMENTS

CAO was supported by the Australian Research Council (ARC) through Discovery Project DP190100252.

FDE acknowledges support by the Science and Technology Facilities Council (STFC), by the ERC through Advanced Grant 695671 'QUENCH', and by the UKRI Frontier Research grant RISE and FALL.

The national facility capability for SkyMapper has been funded through ARC LIEF grant LE130100104 from the Australian Research Council, awarded to the University of Sydney, the Australian National University, Swinburne University of Technology, the University of Queensland, the University of Western Australia, the University of Melbourne, Curtin University of Technology, Monash University, and the Australian Astronomical Observatory. SkyMapper is owned and operated by The Australian National University's Research School of Astronomy and Astrophysics. The survey data were processed and provided by the SkyMapper Team at ANU. The SkyMapper node of the All-Sky Virtual Observatory (ASVO) is hosted at the National Computational Infrastructure (NCI). Development and support of the SkyMapper node of the ASVO has been funded in part by Astronomy Australia Limited (AAL) and the Australian Government through the Commonwealth's Education Investment Fund (EIF) and National Collaborative Research Infrastructure Strategy (NCRIS), particularly the National eResearch Collaboration Tools and Resources (NeCTAR) and the Australian National Data Service Projects (ANDS).

This paper uses data from the VISTA Hemisphere Survey ESO programme ID:179.A-2010 (PI. McMahon). Based on observations obtained as part of the VISTA Hemisphere Survey, ESO Program, 179.A-2010 (PI:McMahon). The VISTA Data Flow System pipeline processing and science archive are described in Irwin et al. (2004), Hambly et al. (2008) and (Cross et al. 2012).

This publication has made use of data from the VIKING survey from VISTA at the ESO Paranal Observatory, programme ID 179.A-2004. Data processing has been contributed by the VISTA Data Flow System at CASU, Cambridge and WFAU, Edinburgh.

The ASKAP radio telescope is part of the Australia Telescope National Facility, which is managed by Australia's national science agency, CSIRO. Operation of ASKAP is funded by the Australian Government with support from the National Collaborative Research Infrastructure Strategy. ASKAP uses the resources of the Pawsey Supercomputing Research Centre. Establishment of ASKAP, the Murchison Radio-astronomy Observatory and the Pawsey Supercomputing Research Centre are initiatives of the Australian Government, with support from the Government of Western Australia and the Science and Industry Endowment Fund. We acknowledge the Wajarri Yamatji people as the traditional owners of the Observatory site. This paper includes archived data obtained through the CSIRO ASKAP Science Data Archive, CASDA (https://data.csiro.au).

The National Radio Astronomy Observatory is a facility of the National Science Foundation operated under cooperative agreement by Associated Universities, Inc. CIRADA is funded by a grant from the Canada Foundation for Innovation 2017 Innovation Fund (Project 35999), as well as by the Provinces of Ontario, British Columbia, Alberta, Manitoba, and Quebec.

DATA AVAILABILITY

The optical quasar data used in this paper come from Onken et al. (2022) with additional quasar data from the Milliquas v7.1 Flesch (2015) found at https://quasars.org/milliquas.htm

The RACS data used in this paper comes from CASDA, which can be accessed through a TAP query of https://casda.csiro.au/casda_vo_tools/tap through the table AS110.racs_dr1_gaussians_galacticcut_v2021_08_v01.

The VLASS data used in this paper comes from the VLASS VizieR Epoch 1 Catalogue, which can be found at https://vizier.cds.unistra.fr/viz-bin/VizieR-3?-source = J/ApJS/255/30/comp

The NVSS data used in this paper came from the NVSS Source catalogue browser, which can be found at https://www.cv.nrao.edu/nvss/NVSSlist.shtml

REFERENCES

Baloković M., Smolčić V., Ivezić Ž., Zamorani G., Schinnerer E., Kelly B. C., 2012, ApJ, 759, 30
Bañados E. et al., 2015, ApJ, 804, 118
Beckwith S. V. W. et al., 2006, AJ, 132, 1729
Bessiere P. S., Tadhunter C. N., Ramos Almeida C., Villar Martín M., 2012, MNRAS, 426, 276
Bischof O. B., Becker R. H., 1997, AJ, 113, 2000
Cirasuolo M., Magliocchetti M., Celotti A., Danese L., 2003, MNRAS, 341, 993
Condon J. J., Cotton W. D., Greisen E. W., Yin Q. F., Perley R. A., Taylor G. B., Broderick J. J., 1998, AJ, 115, 1693
Cross N. J. G. et al., 2012, A&A, 548, A119
de Vries W. H., Becker R. H., White R. L., 2006, AJ, 131, 666
Donoso E., Li C., Kauffmann G., Best P. N., Heckman T. M., 2010, MNRAS, 407, 1078
Edge A., Sutherland W., Kuijken K., Driver S., McMahon R., Eales S., Emerson J. P., 2013, The Messenger, 154, 32

Elvis M. et al., 1994, ApJS, 95, 1
Flesch E. W., 2015, PASA, 32, e010
Floyd D. J. E. et al., 2010, ApJ, 713, 66
Gaia Collaboration et al., 2021, A&A, 649, A1
Goldschmidt P., Kukula M. J., Miller L., Dunlop J. S., 1999, ApJ, 511, 612
Gordon Y. A. et al., 2021, ApJS, 255, 30
Hale C. L. et al., 2021, PASA, 38, e058
Hambly N. C. et al., 2008, MNRAS, 384, 637
Hooper E. J., Impey C. D., Foltz C. B., Hewett P. C., 1995, ApJ, 445, 62
Hopkins P. F., Hernquist L., Cox T. J., Di Matteo T., Robertson B., Springel V., 2006, ApJS, 163, 1
Irwin M. J. et al. Society of Photo-Optical Instrumentation Engineers (SPIE), 2004, in Quinn P. J., Bridger A., eds, SPIE Conf. Ser. Vol. 5493, Optimizing Scientific Return for Astronomy through Information Technologies. SPIE Astronomical Telescopes + Instrumentation, Glasgow, United Kingdom 411
Ivezić Ž. et al., 2002, AJ, 124, 2364
Ivezić Ž. et al., 2004a, in Mújica R., Maiolino R., eds, Multiwavelength AGN Surveys. World Scientific Publishing Co. Pte. Ltd., Singapore, p. 53
Ivezić Z. et al., 2004b, in Richards G. T., Hall P. B., eds, ASP Conf. Ser. Vol. 311, AGN Physics with the Sloan Digital Sky Survey. Astron. Soc. Pac., San Francisco, p. 347
Jiang L., Fan X., Ivezić Ž., Richards G. T., Schneider D. P., Strauss M. A., Kelly B. C., 2007, ApJ, 656, 680
Kalfountzou E., Jarvis M. J., Bonfield D. G., Hardcastle M. J., 2012, MNRAS, 427, 2401
Kellermann K. I., Sramek R., Schmidt M., Shaffer D. B., Green R., 1989, AJ, 98, 1195
Khochfar S., Burkert A., 2003, ApJ, 597, L117
Kratzer R. M., Richards G. T., 2015, AJ, 149, 61
La Franca F., Gregorini L., Cristiani S., de Ruiter H., Owen F., 1994, AJ, 108, 1548
Lacy M., Laurent-Muehleisen S. A., Ridgway S. E., Becker R. H., White R. L., 2001, ApJ, 551, L17
Lin L. et al., 2008, ApJ, 681, 232
Liu Y. et al., 2021, ApJ, 908, 124
Macfarlane C. et al., 2021, MNRAS, 506, 5888
Mandelbaum R., Li C., Kauffmann G., White S. D. M., 2009, MNRAS, 393, 377
Marocco F. et al., 2021, ApJS, 253, 8
Matthews T. A., Sandage A. R., 1963, ApJ, 138, 30
McConnell D. et al., 2020, PASA, 37, e048
McMahon R. G., Banerji M., Gonzalez E., Koposov S. E., Bejar V. J., Lodieu N., Rebolo R., VHS Collaboration 2013, The Messenger, 154, 35
Miller L., Peacock J. A., Mead A. R. G., 1990, MNRAS, 244, 207
Onken C. A. et al., 2019, PASA, 36, e033
Onken C. A., Wolf C., Bian F., Fan X., Hon W. J., Raithel D., Tisserand P., Lai S., 2022, MNRAS, 511, 572
Padovani P., 1993, MNRAS, 263, 461
Peacock J. A., Miller L., Longair M. S., 1986, MNRAS, 218, 265
Rees G. A. et al., 2016, MNRAS, 455, 2731
Retana-Montenegro E., Röttgering H. J. A., 2017, A&A, 600, A97
Richards G. T. et al., 2006, ApJS, 166, 470
Rusinek K., Sikora M., Kozieł-Wierzbowska D., Gupta M., 2020, ApJ, 900, 125
Rusinek-Abarca K., Sikora M., 2021, ApJ, 922, 202
Sandage A., 1965, ApJ, 141, 1560
Schlegel D. J., Finkbeiner D. P., Davis M., 1998, ApJ, 500, 525
Schmidt M., 1963, Nature, 197, 1040
Schneider D. P., van Gorkom J. H., Schmidt M., Gunn J. E., 1992, AJ, 103, 1451
Shang Z. et al., 2011, ApJS, 196, 2
Shankar F. et al., 2016, ApJ, 818, L1
Shen Y., 2009, ApJ, 704, 89
Singal J., Petrosian V., Lawrence A., Stawarz Ł., 2011, ApJ, 743, 104
Singal J., Petrosian V., Stawarz Ł., Lawrence A., 2013, ApJ, 764, 43
Skrutskie M. F. et al., 2006, AJ, 131, 1163
Stern D., Djorgovski S. G., Perley R. A., de Carvalho R. R., Wall J. V., 2000, AJ, 119, 1526
Stocke J. T., Morris S. L., Weymann R. J., Foltz C. B., 1992, ApJ, 396, 487
Tadhunter C., 2016, A&A Rev., 24, 10
Treister E., Schawinski K., Urry C. M., Simmons B. D., 2012, ApJ, 758, L39
Visnovsky K. L., Impey C. D., Foltz C. B., Hewett P. C., Weymann R. J., Morris S. L., 1992, ApJ, 391, 560
White R. L., Helfand D. J., Becker R. H., Glikman E., de Vries W., 2007, ApJ, 654, 99
Wolf C. et al., 2018, PASA, 35, e010
Wright E.L., 2010, AJ, 140, 1868
Wylezalek D. et al., 2013, ApJ, 769, 79
Yang J. et al., 2016, ApJ, 829, 33

This paper has been typeset from a TEX/LATEX file prepared by the author.